

A global climatology of stratospheric OCIO

C. Tétard et al.

This discussion paper is/has been under review for the journal Atmospheric Measurement Techniques (AMT). Please refer to the corresponding final paper in AMT if available.

A global climatology of stratospheric OCIO derived from GOMOS measurement

C. Tétard¹, D. Fussen¹, F. Vanhellemont¹, C. Bingen¹, E. Dekemper¹,
N. Mateshvili¹, D. Pieroux¹, C. Robert¹, E. Kyrölä², J. Tamminen², V. Sofieva²,
A. Hauchecorne³, F. Dalaudier³, J.-L. Bertaux³, O. Fanton d'Andon⁴, G. Barrot⁴,
L. Blanot⁴, A. Dehn⁵, and L. Saavedra de Miguel⁶

¹Institut d'Aéronomie Spatiale de Belgique, Brussels, Belgium

²Finnish Meteorological Institute, Earth Observation, Helsinki, Finland

³Laboratoire Atmosphères, Milieux, Observations Spatiales, CNRS-INSU,
Univ. Versailles St-Quentin, Guyancourt, France

⁴ACRI-ST, Sophia-Antipolis, France

⁵European Space Research Institute (ESRIN), European Space Agency, Frascati, Italy

⁶IDEAS, Serco, Frascati, Italy

Received: 27 February 2013 – Accepted: 3 April 2013 – Published: 11 April 2013

Correspondence to: C. Tétard (cedric.tetard@aeronomie.be)

Published by Copernicus Publications on behalf of the European Geosciences Union.

Title Page

Abstract

Introduction

Conclusions

References

Tables

Figures

◀

▶

◀

▶

Back

Close

Full Screen / Esc

Printer-friendly Version

Interactive Discussion



Abstract

The Global Ozone Monitoring by Occultation of Stars (GOMOS) instrument on board the European platform ENVISAT was dedicated to the study of the atmosphere of the Earth using the stellar occultation technique. The spectral range of the GOMOS spectrometer extends from the UV to the near infrared, allowing for the retrieval of species such as O₃, NO₂, NO₃, H₂O, O₂, air density, aerosol extinction and OCIO. Nevertheless, OCIO can not be retrieved using a single GOMOS measurement because of the weak signal-to-noise ratio and the small optical thickness associated with this molecule. We present here the method used to detect this molecule by using several GOMOS measurements. It is based on a two-step approach. First, several co-located measurements are combined in a statistical way to build an averaged measurement with a higher signal-to-noise ratio. Then, a Differential Optical Absorption Spectroscopy (DOAS) method is applied to retrieve OCIO slant column densities. The statistics of the sets of GOMOS measurements used to build the averaged measurement and the spectral window selection are analyzed. The obtained retrievals are compared to results from two balloon-borne instruments. It appears that the inter-comparisons of OCIO are generally satisfying. Then, two nighttime climatologies of OCIO slant column densities based on GOMOS averaged measurements are presented. The first depicts annual global pictures of OCIO from 2003 to 2011. From this climatology, the presence of an OCIO layer in the equatorial region at about 35 km is confirmed and strong concentrations of OCIO in both polar regions are observed, a sign of chlorine activation. The second climatology is a monthly time series. It clearly shows the chlorine activation of the lower stratosphere during winter. Moreover the equatorial OCIO layer is observed during all the years without any significant variations. Finally, the anti-correlation between OCIO and NO₂ is highlighted. This very promising method, applied on GOMOS measurements, allowed us to build the first nighttime climatology of OCIO.

AMTD

6, 3511–3543, 2013

A global climatology of stratospheric OCIO

C. Tétard et al.

Title Page

Abstract

Introduction

Conclusions

References

Tables

Figures

◀

▶

◀

▶

Back

Close

Full Screen / Esc

Printer-friendly Version

Interactive Discussion



1 Introduction

The discovery of the stratospheric ozone depletion in Antarctica by Farman et al. (1985) has led to numerous studies to understand the physico-chemical mechanisms involved in this recurrent phenomenon. It appears that the halogen species play an important role in the chemical cycles that lead to polar ozone depletion (Solomon et al., 1986). Of these cycles, those involving active chlorine species (Cl, ClO, Cl₂O₂) are among the most efficient (Salawitch et al., 1993). The presence of chlorine species in the atmosphere is mainly due to the emission of chlorofluorocarbons (CFC) at the ground. CFCs are chemically inert in the troposphere and are not soluble in water, which make them resistant to washout processes. Therefore, they are efficiently transported toward the stratosphere where they are photolyzed by UV radiation or oxidized to produce atomic chlorine and chlorine monoxide (ClO). One consequence of the accumulation of ClO in the stratosphere is the formation of chlorine dioxide (OCIO) via one of the possible reactions between ClO and bromine dioxide (BrO):



Thus, the detection of OCIO in the stratosphere is a sign of chlorine activation. Also, nitrogen dioxide (NO₂) is of primary importance for polar ozone chemistry. Notably, in the presence of a third molecule (for example N₂ or O₂), NO₂ reduces the production of OCIO by reacting with ClO or BrO to form inert chlorine and bromine reservoirs:



During the night, NO₂ reacts with nitrogen trioxide (NO₃) to form dinitrogen pentoxide (N₂O₅). The nighttime formation of N₂O₅ is responsible for the slow decrease of NO₂

Title Page

Abstract

Introduction

Conclusions

References

Tables

Figures

◀

▶

◀

▶

Back

Close

Full Screen / Esc

Printer-friendly Version

Interactive Discussion



A global climatology of stratospheric OCIO

C. Tétard et al.

Title Page

Abstract

Introduction

Conclusions

References

Tables

Figures

◀

▶

◀

▶

Back

Close

Full Screen / Esc

Printer-friendly Version

Interactive Discussion



and NO_3 during the night. Therefore in the permanent night of high latitudes regions, this reaction leads to the removal of almost all of NO_2 and NO_3 : this is the well-known denoxification process. Subsequently, Reactions (R4) and (R5) are very limited in the polar vortex and OCIO can then be formed via the Reaction (R1). Consequently, OCIO and NO_2 are expected to be anti-correlated in the polar regions. The OCIO concentration is expected to remain constant during the night as the only sink of this species is the photolysis by the solar radiation. The absorption cross-section of OCIO is characterized by strong differential structures in the near UV-range. This feature will also allow us to perform the retrieval of OCIO. More details about stratospheric chemical processes involving chlorine and nitrogen species can be found in Solomon (1999).

Another important aspect of the OCIO chemistry is its interactions with NO_2 which are not completely understood. A few studies have covered the subject (Riviere et al., 2003, 2004; Berthet et al., 2007; Tétard et al., 2009) but all have concluded that uncertainties in the understanding of these interactions persist. It is therefore critical to monitor simultaneously OCIO and NO_2 . Although NO_2 monitoring in the stratosphere has been extensively tackled by the scientific community, OCIO monitoring has been much less so. For example, we can mention the studies of the vertical column of OCIO retrieved using ground-based instruments (Solomon et al., 1987; Miller et al., 1999) or using nadir-viewing satellite instruments: GOME (Wagner et al., 2002), SCIAMACHY (Oetjen et al., 2011). Also, the vertical profiles of OCIO concentration have been retrieved during nighttime using balloon-borne instruments: Absorption by the Minor components Ozone and Nox (AMON, Renard et al., 1997) and Spectroscopie d’Absorption Lunaire pour l’Observation des Minoritaires Ozone et NO_x (SALOMON, Renard et al., 2000). In this study, flights of these two instruments have been used to validate the OCIO concentration profiles retrieved from the Global Ozone Monitoring by Occultation of Stars (GOMOS) measurements (Bertaux et al., 2010). Also, some satellite instruments are used to retrieve the vertical distributions of OCIO using limb-scattered sunlight measurements: Optical Spectrograph and InfraRed Imager System (OSIRIS; Krecl et al., 2006) and SCIAMACHY (Kühl et al., 2008). Finally, the

Stratospheric Aerosol and Gas Experiment III (SAGE III) instrument is also able to retrieve OCIO vertical profiles using its lunar occultation mode but no scientific studies about this have been published yet.

GOMOS is the only satellite instrument able to perform nighttime measurements of the vertical distribution of OCIO on a long term and on a global scale. Two previous studies about OCIO retrieved using measurements from the GOMOS instrument have already been published: the first by Fussen et al. (2006) has demonstrated the ability to retrieve OCIO and has discovered the presence of an equatorial OCIO layer in the upper stratosphere and the second by Tétard et al. (2009) has illustrated the anti-correlation between OCIO and NO_2 in the Arctic polar vortex only for winters 2003 to 2008. Nevertheless, no extended climatology of stratospheric OCIO from GOMOS has yet been published.

In this paper, we present the method used to retrieve OCIO from GOMOS measurements. The method is an evolution of that described in Fussen et al. (2006). A more careful statistical processing has been applied and the spectral window has been optimized. Firstly, a statistical analysis is applied on several co-located GOMOS transmittance measurements to construct an averaged transmittance measurement. Then, a DOAS process based on these averaged measurements is applied to compute slant column density (hereafter SCD) of OCIO. Then, the study focuses on the validation of the OCIO GOMOS products by inter-comparisons with those retrieved from two different balloon-borne measurements. Finally, global annual and monthly climatologies of OCIO are presented and the anti-correlation between NO_2 and OCIO is highlighted.

This article focuses on the importance and the power of the use of averaged measurements to detect small absorbers.

2 The GOMOS instrument

The GOMOS instrument has been embarked on the European platform ENVISAT (Environment SATellite) in February 2002 on a heliosynchronous orbit at 800 km altitude

A global climatology of stratospheric OCIO

C. Tétard et al.

Title Page

Abstract

Introduction

Conclusions

References

Tables

Figures

◀

▶

◀

▶

Back

Close

Full Screen / Esc

Printer-friendly Version

Interactive Discussion



A global climatology of stratospheric OCIO

C. Tétard et al.

[Title Page](#)[Abstract](#)[Introduction](#)[Conclusions](#)[References](#)[Tables](#)[Figures](#)[◀](#)[▶](#)[◀](#)[▶](#)[Back](#)[Close](#)[Full Screen / Esc](#)[Printer-friendly Version](#)[Interactive Discussion](#)

and with an inclination of 98.55° . The GOMOS mission ended on April 2012 when contact with ENVISAT was lost. During its ten years of operation, GOMOS carried out about 860 000 occultations. The instrument operation is based on a grating spectrometer operating in stellar occultation mode: at each tangent altitude z and each wavelength λ , the transmittance $T(\lambda, z)$ is obtained by dividing the stellar radiance attenuated through the atmosphere $S(\lambda, z)$ by the reference star radiance $S_0(\lambda)$ measured outside the atmosphere. Thus, these measurements are self-calibrated and this is one of the main advantages of the method. Another advantage is related to the important number of light sources available (about 180 stars are used) that allows a global coverage in about 3 days (according to the mission baseline scenario). Nevertheless, some drawbacks of the stellar occultation method have to be mentioned. The selected stars have different magnitude, temperature and spectra with a clear impact on the signal-to-noise ratio of the measured spectra and therefore on the retrieval error budget. Moreover, the scintillation of stars has to be considered (Bertaux et al., 1988). It is due to small-scale vertical temperature fluctuations of the atmosphere. To overcome this problem, two fast photometers (with 1 kHz sampling rate) were installed in parallel to the spectrometers. However, it appears that the correction of the scintillation is right when the star setting is vertical (close to the orbital plane) but imperfect for oblique occultations (Sofieva et al., 2009). In this case, residual scintillation persists due to atmospheric inhomogeneous horizontal structures. Figure 1 shows an example of transmittance spectra obtained from oblique (top panel) and vertical (middle panel) occultations. The presence of residual scintillations is clearly visible in the spectra from oblique occultation whereas scintillation is almost perfectly removed in the spectra from vertical occultation. The vertical resolution is 1.7 km for vertical occultations and better for oblique ones.

GOMOS is in fact made of four spectrometers: the two first in the UV-visible spectral range (from 250 to 675 nm with a spectral resolution of 0.8 nm), the third in the 756 to 773 nm range (with 0.13 nm resolution) and the last in the near infrared (926 to 952 nm with a spectral resolution of 0.13 nm). The main goal of GOMOS is the global, long term

monitoring of stratospheric and mesospheric ozone. Furthermore, the large wavelength range and the spectral resolutions allows the retrieval of other species like NO₂, NO₃, H₂O, O₂, OCIO and aerosol extinction (Bertaux et al., 2010). The following section explains the method used to retrieve OCIO.

3 The retrieval of OCIO

The starting point of most occultation retrieval algorithm is the well-known Beer-Lambert law. It describes how the signal is affected by the presence of atmospheric absorbers along the line of sight at tangent altitude z :

$$S(\lambda, z) = S_0(\lambda) \exp \left(- \sum_i \sigma_i(\lambda) N_i(z) \right) \quad (1)$$

where σ_i is the extinction cross-section and N_i is the slant column density of each atmospheric absorbers in the spectral range selected. A detailed overview of the GOMOS operational algorithm can be find in Kyrölä et al. (2010b). Most of the expected species can be directly retrieved from single measurements but the combination of the weak signal-to-noise ratio of a single GOMOS measurement and the small optical thickness of OCIO forces us to combine several single measurements in order to detect it. The retrieval of OCIO from GOMOS measurements requires two steps. The first is the calculation of an averaged transmittance spectra and the second is the inversion process of these spectra.

As written previously, the first step is required to increase the signal-to-noise ratio so that the retrieval of OCIO can be carried out in the second step of the process. The idea is to use several co-located (spatially and temporally) GOMOS measurements to build a new measurement. This is possible because each measurements consists of a transmittance and is consequently independent of the selected star. This averaged measurement is supposed to be representative of one particular location for a given

Title Page

Abstract

Introduction

Conclusions

References

Tables

Figures

◀

▶

◀

▶

Back

Close

Full Screen / Esc

Printer-friendly Version

Interactive Discussion



moment. For the selection of the GOMOS measurements used to build the averaged measurements, we have used the following steps:

- selection of stars: stars with effective temperatures greater than 4100 K to ensure a sufficient UV flux and stars with magnitudes lower than 2 to have acceptable photon fluxes. These criteria lead to a selection of 44 stars.
- temporal resolution: one month or one year. The time period is September 2002 to the end of 2011. The choice of this temporal bin size is influenced by the latitudinal resolution hereafter.
- latitude bands: for the annual climatologies, we have used 10° latitude bands and for the monthly time series, we have used 20° latitude bands for the regions located between -30° and +30° and 30° latitude bands elsewhere to ensure sufficient numbers of measurements in each data set.
- illumination conditions: only dark limb and straylight condition measurements are used. Dark limb condition corresponds to measurements made when the solar zenith angle is higher than 120°. These measurements are supposed to be used without restriction. Measurements are said to be in straylight conditions if the instrument is illuminated by light coming from the scattering of solar light. Straylight measurements are considered as of good quality (more details can be found in the GOMOS product handbook at <http://envisat.esa.int/handbooks/gomos/toc.htm>).
- the GOMOS data used here are obtained with the version 5 of the ESA level 1 operational processor.
- all the selected spectra are linearly interpolated on a common vertical grid of tangent altitudes from 0 to 60 km with 1 km step.

Figure 2 shows the latitudinal distribution of the GOMOS data used in our study. A total number of about 162 000 GOMOS measurements has been processed. While both polar regions are well covered during the winters and much less outside these

A global climatology of stratospheric OCIO

C. Tétard et al.

Title Page

Abstract

Introduction

Conclusions

References

Tables

Figures

◀

▶

◀

▶

Back

Close

Full Screen / Esc

Printer-friendly Version

Interactive Discussion



periods, the other latitudes are very well sampled during all years (except in 2005). During the first months of 2005 (until June), almost no measurements are available due to an instrumental breakdown. However, some measurements in the polar regions could be carried out (particularly in January).

For each bin, we have built a data set: $[T_1(\lambda_i, z_j), \dots, T_n(\lambda_i, z_j)]$ where z_j are the 61 tangent altitude levels, λ_i are the wavelengths and n is the number of GOMOS measurements in the bin. Once all the data sets are built, they should be statistically analyzed to guarantee the homogeneity of the bin data sets and subsequently, to ensure the representativity of the averaged measurement that will be derived from this data set. For each data set, statistical detections of multimodal distribution are performed by fitting the distribution with theoretical models. Figure 3 shows examples of GOMOS transmittance distributions for a monomodal and a bimodal case. The bimodality observed here in the high latitude band is due to the fact that some measurements are inside the polar vortex and others are outside. In fact, transmittances inside the polar vortex are greater than those outside the polar vortex because the decrease in NO_2 concentrations in the vortex area (denoxification) is not sufficiently offset by the increase of OCIO concentrations. All the cases of bimodal distributions observed in our study are due to measurements done inside and outside the polar vortex. In this case, both modes are studied separately and, after visual inspection, we have selected the one that represents the high latitude band, in other words the one inside the polar vortex with greater transmittances (the other modes will be analyzed in the frame of some case studies). Then, an outlier detection is performed for each dataset using a jackknife method. Finally, for each tangent altitude and each wavelength, the weighted median transmittance is calculated. A weighted median calculation starts by sorting the transmittance values in increasing order, and rearranging the associated weights in the same fashion. The cumulative distribution of these weights is subsequently evaluated. The weighted median is then the transmittance value corresponding to the 50 % level of this cumulative weight distribution. The uncertainty associated with the weighted median is calculated as the weighted median absolute deviation (WMAD). It is the median

A global climatology of stratospheric OCIO

C. Tétard et al.

Title Page

Abstract

Introduction

Conclusions

References

Tables

Figures

◀

▶

◀

▶

Back

Close

Full Screen / Esc

Printer-friendly Version

Interactive Discussion



A global climatology of stratospheric OCIO

C. Tétard et al.

Title Page

Abstract

Introduction

Conclusions

References

Tables

Figures

◀

▶

◀

▶

Back

Close

Full Screen / Esc

Printer-friendly Version

Interactive Discussion



of the absolute values of the difference between each transmittance values and the weighted median. This statistical study ensures that the calculated averaged spectra are representative of the considered region. Figure 1 shows transmittance spectra in the 250 to 690 nm range for a single oblique occultation, a single vertical occultation and an averaged occultation. We can note that the signs of residual scintillation disappear in the averaged spectra (bottom panel) and that residual scintillations are almost perfectly corrected in the vertical occultation spectra (center panel) whereas some remaining scintillations persist in the oblique spectra (top panel).

The second step consists of a Differential Optical Absorption Spectroscopy (DOAS) algorithm applied to averaged transmittance spectra to retrieve all the chemical species involved in the absorption of the radiation in the wavelength range used. The DOAS technique has been reviewed by Platt et al. (1979). The principle of this method is quite simple: it is based on the idea that the transmittance consists of two components, one varying slowly with the wavelength and the other rapidly varying. In the spectral range used, the slowly varying component $T_s(\lambda)$ reflects the Rayleigh scattering, aerosol extinction and the slowly varying part of the gaseous absorptions while the second component represents the rapidly varying part of gaseous absorptions. $T_s(\lambda)$ is obtained by fitting the measured transmittance $T(\lambda)$ by a second order polynomial in the wavelength window selected. Then, the experimental differential transmittance $dT(\lambda)$ is simply expressed as the difference between $T(\lambda)$ and $T_s(\lambda)$ while the modeled differential transmittance $M(\lambda)$ is expressed as:

$$M(\lambda) = T_s \left(\exp \left[- \sum_j N_{\text{gas}_j} \delta \sigma_{\text{gas}_j} \right] - 1 \right) \quad (2)$$

where N_{gas_j} and $\delta \sigma_{\text{gas}_j}$ correspond respectively to the SCD and the differential cross-sections of the absorber gas in the wavelength interval. $\delta \sigma_{\text{gas}_j}$ is the difference between the absorption cross-section of gas j and a first order polynomial fitting this cross-section. Using Eq. (2), a nonlinear least-square minimization between the

modeled and the experimental differential transmittances weighted by the measurement errors is applied for each tangent altitude to obtain the SCD of each species contributing to the absorption in the selected wavelength range and the retrieval errors (extracted from the jacobian matrix). We have studied 4 spectral ranges: 355–381 nm, 355–390 nm, 390–425 nm and 355–425 nm. For these 4 fitting windows, we have calculated at each tangent altitude z_t the reduced chi-square χ^2 :

$$\chi^2(z_t) = \frac{1}{d_f} \sum_{i=1}^n \left[\frac{dT(\lambda_i, z_t) - M(\lambda_i, z_t)}{\epsilon(\lambda_i, z_t)} \right]^2. \quad (3)$$

In this expression, n is the number of pixels in the fitting window, d_f is the degree of freedom (n minus the number of parameters used in the minimization process) and ϵ is the error associated to the averaged differential transmittance. For the fitting windows selected, the reduced chi-square are between about 0.1 and 1.5 (an example is presented in the top left panel in Fig. 4). On the basis of this example, the best chi-square ($\chi^2 \approx 1$) is obtained with the interval 355–381 nm for all the altitude range. Moreover, the analysis of the mean of the residual (i.e. the difference between observed and modeled transmittances) at each tangent altitude shows that below 25 km there is almost no differences but above, the mean residual is lower when the 355–381 nm wavelength range is used (bottom left panel in Fig. 4). Furthermore, residuals at each tangent altitude (right panels in Fig. 4) are clearly smaller below 390 nm. The same study has been done using several other averaged occultations and the conclusions are always identical: we have therefore selected the 355–381 nm spectral window. In this spectral range, we have to consider the absorptions of OCIO, NO₂ and also O₃ even if its cross-section is very small in this range. Thus, these 3 species are fitted simultaneously. In Fig. 5, we show an example of OCIO SCDs in the Antarctic region (in blue), in the Arctic region (in black) and in the equatorial region (in red) for the year 2003. For OCIO, the retrieval errors are generally better than 50%. We can already notice several specific structures that will be discussed in more detail in the following sections. In particular, we can observe the presence of an “OCIO layer” in the middle stratosphere

A global climatology of stratospheric OCIO

C. Tétard et al.

Title Page	
Abstract	Introduction
Conclusions	References
Tables	Figures
◀	▶
◀	▶
Back	Close
Full Screen / Esc	
Printer-friendly Version	
Interactive Discussion	



Discussion Paper | Discussion Paper | Discussion Paper | Discussion Paper | Discussion Paper

in the equatorial regions and the expected chlorine activation in the lower stratosphere in both polar regions with a higher amplitude in the south.

The following section presents a preliminary validation of the OCIO GOMOS product by comparisons with products retrieved using balloon-borne instruments.

4 Comparisons with other instruments

Since the nighttime OCIO SCD from GOMOS averaged measurements is a new product, it is not easy to validate it. In this validation exercise, we have excluded O₃ and NO₂ SCDs retrieved using the present algorithm because the spectral window used is not the most appropriate one to perform the retrieval of these species, considered here as interfering species. Nonetheless, as a first analysis of the quality of our products, we can compare NO₂ retrieved from GOMOS averaged measurements and the operational GOMOS data. This has been done previously and published in Tétard et al. (2009). The results (not reproduced here) indicate that there is a very good agreement between both products (typically, relative differences are between -10 and 10%) and that our method seems to work properly.

The second step consists in comparing the GOMOS products with those from other instruments. The only nighttime OCIO concentration profiles available for comparisons are those retrieved from the AMON and SALOMON balloon-borne instruments. One should keep in mind that these comparisons are done between spatially and temporally localized measurements and a composite of several measurements localized in a latitude band. AMON and SALOMON instruments performed nighttime remote sensing measurements using respectively the stellar and the lunar occultation method. They provided slant column densities of OCIO. However, since the observation geometries of GOMOS and of balloon-borne instruments are different, it is not appropriate to compare directly the slant column densities but instead should compare the OCIO vertical profiles. To do so, we had to perform spatial inversion of the SCDs. For GOMOS, this has been done by using an onion peeling method. The atmosphere is divided into

Title Page

Abstract

Introduction

Conclusions

References

Tables

Figures

◀

▶

◀

▶

Back

Close

Full Screen / Esc

Printer-friendly Version

Interactive Discussion



concentric layers that are assumed to be homogeneous. Using the matrix formalism, the problem consists of solving the following linear system:

$$\mathbf{N} = \mathbf{K}\mathbf{n} \quad (4)$$

where the matrix elements of \mathbf{N} are the OCIO SCDs at each tangent altitude, \mathbf{K} is the kernel matrix (a triangular square matrix) and \mathbf{n} is the OCIO vertical profiles matrix. The GOMOS spatial inversion is a well-conditioned problem and is easy to solve by using standard method.

AMON is a UV-visible spectrometer that uses the stellar occultation method. The flight used took place in March 2003 in Kiruna, northern Sweden (latitude $67^{\circ}53' \text{ N}$, longitude $21^{\circ}05' \text{ E}$). We have used the measurements from the occultation of Sirius (α Canis Majoris) and Alnilam (ϵ Orionis). Both stars emit enough UV radiation to detect OCIO (effective temperatures are respectively 11 000 and 30 000 K).

The second balloon-borne instrument used is SALOMON (Renard et al., 2000). It is a UV-visible spectrometer that uses the lunar occultation method. The flight occurred in January 2006 in Kiruna and the measurements were done during the balloon ascent inside the polar vortex. The OCIO concentration profile from the SALOMON measurements has been studied by comparisons with the results of the model described in Berthet et al. (2007). In particular, they have shown that OCIO product from SALOMON is in an acceptable agreement with results from chemistry transport model calculations.

For the inter-comparisons, the GOMOS measurements used to build the averaged measurements were chosen located between 60° and 75° and took place in a 20 days window centered on the flight date. Since the GOMOS vertical resolution is close to the AMON and SALOMON resolutions, no smoothing procedure was required and direct comparisons could be done.

Figure 6 shows the OCIO concentration profiles comparisons. The curves on the left concern the comparisons with AMON and show a satisfactory agreement. The maxima are reached at approximately the same altitudes for the three profiles (19 km). The value of the maximum of OCIO concentrations are almost identical for the GOMOS and

A global climatology of stratospheric OCIO

C. Tétard et al.

Title Page

Abstract

Introduction

Conclusions

References

Tables

Figures

◀

▶

◀

▶

Back

Close

Full Screen / Esc

Printer-friendly Version

Interactive Discussion



A global climatology of stratospheric OCIO

C. Tétard et al.

Title Page

Abstract

Introduction

Conclusions

References

Tables

Figures

◀

▶

◀

▶

Back

Close

Full Screen / Esc

Printer-friendly Version

Interactive Discussion



the AMON (ϵ -ORI) profiles but is higher for the AMON (α -CMA) profile: $5.3 \times 10^7 \text{ cm}^{-3}$, $5 \times 10^7 \text{ cm}^{-3}$ and $1 \times 10^8 \text{ cm}^{-3}$ respectively. The differences in concentration could be explained by asserting that the OCIO concentrations can vary according to the area of the vortex observed. A secondary maximum is observed in the three profiles at almost the same altitudes: 26 km for GOMOS and AMON (ϵ -ORI) and 26.5 km for AMON (α -CMA). Here again, the concentration values reached are almost identical for the GOMOS and the AMON (ϵ -ORI) profiles (respectively 1.6×10^7 and $1.8 \times 10^7 \text{ cm}^{-3}$) whereas the AMON (α -CMA) profile exhibits a higher value: $2.5 \times 10^7 \text{ cm}^{-3}$. Overall, the OCIO profile from the GOMOS averaged measurement is closer to the product of AMON when ϵ -ORI is occulted: for the entire altitude range, the AMON (ϵ -ORI) profiles are well within the GOMOS error bars.

Concerning the comparisons with SALOMON (right panel of Fig. 6), the agreement is moderate. The first maximum is reached at about 20 km for SALOMON and at 18 km for GOMOS. This difference may not be significant because of the vertical resolution of SALOMON for this product (2 km). However, the maximum of OCIO concentration measured by SALOMON is twice the one retrieved by GOMOS (1.2×10^8 and $6.1 \times 10^7 \text{ cm}^{-3}$ respectively). Moreover, above 28 km, the SALOMON concentrations increase strongly reaching a value of $1.3 \times 10^8 \text{ cm}^{-3}$ at 32 km whereas the OCIO concentrations from GOMOS are always decreasing.

In summary, the OCIO product from GOMOS averaged measurements compares very well with that from AMON measurements and slightly less well with that of SALOMON. Overall, the conclusion is that our OCIO retrieval is of sufficient quality for scientific use.

5 Climatology of OCIO

5.1 Annual climatology

As specified previously, we use 10° latitude bins for the annual climatologies. For each altitude, the distribution of OCIO SCDs with latitude are fitted by one or two lorentzian function(s), taking into account the retrieval errors.

In Fig. 7, we present the isopleths of the latitude-altitude OCIO slant column densities (log scales) for years 2003 to 2011. The altitude range is limited from 15 to 45 km. Outside this range, either the retrieval does not succeed or the uncertainties of the retrieval are too large. The 9 latitude-altitude maps of OCIO SCDs presented in Fig. 7 show approximately the same structure. In the lower stratosphere, we can observe high values in the polar regions, reaching about 10^{16} cm^{-2} in the southern hemisphere and generally slightly less in the north (about 10^{15} cm^{-2}). These high values are expected (Eq. R1) and are an indication of the chlorine activation that occurs in spring (in the northern hemisphere) and in fall (in the southern hemisphere). At higher altitude in the polar regions, OCIO SCDs decrease abruptly for all years. This decrease can be explained by the scarcity of ClO at these altitudes. This is well observed by the Microwave Limb Sounder (MLS) instrument onboard the satellite platform AURA (see plots available at <http://mls.jpl.nasa.gov>).

In the equatorial region, an OCIO layer is present all year between about 30 to 35 km. The latitudinal extent as well as the maxima of the layer is somewhat variable from one year to another. The fact remains that the maxima are about a few 10^{14} cm^{-2} . The location of the maxima is approximately around the equator. Note that the year 2011 exhibits the stronger OCIO equatorial layer (the maxima is nearly 10^{15} cm^{-2}). The OCIO equatorial stratospheric layer was first discovered by Fussen et al. (2006) for the year 2003. A possible explanation for the presence of OCIO at these altitudes can be the low pressure at these levels which make the 3 body reactions between ClO/BrO and NO_2 (Reactions R4 and R5) less effective. Thus, the Reaction (R1) between ClO and BrO become dominant and explain the presence of OCIO. Moreover, the satellite instrument

Title Page

Abstract

Introduction

Conclusions

References

Tables

Figures

◀

▶

◀

▶

Back

Close

Full Screen / Esc

Printer-friendly Version

Interactive Discussion



MLS confirms the presence of a ClO layer in the upper stratosphere in the equatorial region. One may notice the more extended (in terms of altitude) OCIO layers for the years 2008 and 2011. Finally, the OCIO SCDs decrease progressively above this layer. The other latitude regions are characterized by weak OCIO values. Consequently, in the following, our attention will be focused on equatorial and polar regions.

5.2 Monthly climatology of OCIO

In Fig. 8, we show the time series of OCIO SCDs in three latitude bands: the equatorial band (10° S–10° N, middle panel), the north polar band (60° N–90° N, top panel) and the south polar band (60° S–90° S, bottom panel). In the equatorial region, the missing data in 2005 are due to a GOMOS failure. The discontinuity observed in the two polar time series are due to the spatial coverage of GOMOS at these altitudes (cf. Fig. 2).

Regarding the northern latitude band, we can clearly observe an annual increase of OCIO followed by a decrease in the lower stratosphere (below about 25 km). The increase begins in December and reaches a maximum of about $5 \times 10^{15} \text{ cm}^{-2}$ to $3 \times 10^{16} \text{ cm}^{-2}$. The corresponding OCIO concentrations (obtained after the spatial inversion described in Sect. 4) are 5×10^7 to $9 \times 10^7 \text{ cm}^{-3}$. This is in good agreement with the values previously observed with other instruments (summarized in Table 1). Regarding the altitude of the maximum of OCIO concentrations, the values obtained using GOMOS measurements (about 17 km) are generally lower than those found by the balloon-borne instruments. The high OCIO values are the sign of chlorine activation in the winter polar vortex. Note that the year 2011 shows strong OCIO values in the lower stratosphere. Indeed, the ozone depletion in the Arctic winter 2010/2011 has been one of the most important of the last decade (Kuttippurath et al., 2012). This feature is also observed in the corresponding annual isopleth (Fig. 7). Figure 9 shows the anti-correlation plot between OCIO and NO_2 concentrations (from the GOMOS operational algorithm version 5) in the Arctic region at 17 km. This altitude has been chosen as an example because it corresponds to the altitude of the maximum of OCIO detected by GOMOS. This choice has no qualitative impact on the following discussion.

Title Page

Abstract

Introduction

Conclusions

References

Tables

Figures

◀

▶

◀

▶

Back

Close

Full Screen / Esc

Printer-friendly Version

Interactive Discussion



The correlation coefficient obtained is about -0.75 which confirms the anti-correlation between NO_2 and OCIO. Indeed, during the permanent polar night, NO_2 is removed from the stratosphere because of Reactions (R4) and (R5). Therefore, the reaction of formation of OCIO (Reaction R1) is more active.

For the south polar region (bottom panel in Fig. 8), only a few months of each year can be analyzed (from July to September). Typically, the time series shows high OCIO values from July to September indicating the sign of chlorine activation. The OCIO SCD maximum reached in the Antarctic regions (from 1.5×10^{16} to $5.7 \times 10^{16} \text{ cm}^{-2}$) are larger than those observed in the Arctic regions. This is well illustrated in Fig. 10 showing these OCIO SCD maxima for winters 2003 to 2011. The maximum concentrations range from $7 \times 10^7 \text{ cm}^{-3}$ to $2 \times 10^8 \text{ cm}^{-3}$. Unfortunately, we can not validate our values because of the lack of occultation measurements in the south pole.

The equatorial region (middle panel in Fig. 8) is characterized by an OCIO layer between about 30 to 40 km for each year. There are too few values available in 2005 to discuss this year. In this layer, the maximum is located at about 35 km for the years 2003, 2006, 2007 and 2009 to 2011. For the years 2004 and 2008, the maximum is located slightly lower, around 32 km. This layer appears to be present during the entire year with only small variations. This is in good agreement with the results obtained by the MLS instrument which shows a quasi-constant CIO layer at these altitudes with a volume mixing ratio of 0.3 to 0.4 ppbv, corresponding to concentrations of 2×10^7 to $3 \times 10^7 \text{ cm}^{-3}$. Note that a stronger OCIO layer is observed for periods ranging from late 2006 to early 2009 and at the beginning of 2011. Further studies are needed to analyze and interpret these observations in cooperation with modelers. As expected, almost no OCIO is detected in the lower part of the stratosphere.

A global climatology of stratospheric OCIO

C. Tétard et al.

Title Page

Abstract

Introduction

Conclusions

References

Tables

Figures

◀

▶

◀

▶

Back

Close

Full Screen / Esc

Printer-friendly Version

Interactive Discussion



6 Conclusions

In this article, we have presented an innovative method to retrieve small absorber concentration. This method is applied to the GOMOS measurements to detect OCIO. It consists of the combination of several co-located GOMOS measurements to build one measurement with a higher signal-to-noise ratio. Then a specified algorithm is used to retrieve OCIO slant column densities.

We have compared our results with those obtained using balloon-borne instruments AMON and SALOMON. It appears that our OCIO product is in a very good agreement with the AMON product and compares slightly less well with SALOMON.

We have constructed climatologies of OCIO based on annual binning. It appears clearly that the same structures emerge every year. First, in the polar regions, we systematically observed a strong increase of OCIO in the lower stratosphere. This is related to the activation of the chlorine species in the polar vortex. Moreover, an OCIO layer in the equatorial region is clearly detected each year in the middle stratosphere. This layer is the result of the reaction between BrO and ClO effectively detected at these altitudes by the MLS instrument.

Time series of OCIO SCDs have been built using averaged measurements representative of one month for three latitude bands corresponding to Arctic, Antarctic and equatorial regions. The period of these climatologies is from 2003 to 2012, covering the entire GOMOS mission. It appears that activation of chlorine species is well observed in the winter pole. Furthermore, the OCIO layer in the equatorial middle stratosphere is detected during all the years studied and presents no particular variations. The anti-correlation between OCIO and NO₂ concentrations is well observed.

The next step of these studies will be the use of models to interpret quantitatively the results presented in this article. The method presented here is really promising and could be applied to other instrumental data. In addition, it can be used to detect other weak absorbers such as BrO. The climatology presented in this paper can be

AMTD

6, 3511–3543, 2013

A global climatology of stratospheric OCIO

C. Tétard et al.

Title Page

Abstract

Introduction

Conclusions

References

Tables

Figures

◀

▶

◀

▶

Back

Close

Full Screen / Esc

Printer-friendly Version

Interactive Discussion



considered as the first and only long-term nighttime OCIO climatology that exists at present.

Acknowledgements. This study was funded by the PRODEX/RADIAL (PEA 4000102793) contract under the authority of the Belgian Space Science Office (BELSPO).

5 We thank the AMON and SALOMON science team for giving us the authorization to use their OCIO concentration profiles.

References

10 Bertaux, J. L., Pellinen, R., Simon, P., Chassefière, E., Dalaudier, F., Godin, S., Goutail, F., Hauchecorne, A., Le Texier, H., Mégie, G., Pommereau, J. P., Brasseur, G., Kyrölä, E., Tuomi, T., Korpela, S., Leppelmeier, G., Visconti, G., Fabian, P., Isaksen, S. A., Larsen, S. H., Stordahl, F., Cariolle, D., Lenoble, J., Naudet, J. P., and Scott, N.: GOMOS, proposal in response to ESA EPOP-1, A.O.1, January 1988. 3516

15 Bertaux, J. L., Kyrölä, E., Fussen, D., Hauchecorne, A., Dalaudier, F., Sofieva, V., Tamminen, J., Vanhellefont, F., Fanton d'Andon, O., Barrot, G., Mangin, A., Blanot, L., Lebrun, J. C., Pérot, K., Fehr, T., Saavedra, L., Leppelmeier, G. W., and Fraisse, R.: Global ozone monitoring by occultation of stars: an overview of GOMOS measurements on ENVISAT, *Atmos. Chem. Phys.*, 10, 12091–12148, doi:10.5194/acp-10-12091-2010, 2010. 3514, 3517

20 Berthet, G., Renard, J. B., Catoire, V., Chartier, M., Robert, C., Huret, N., Coquelet, F., Bourgeois, Q., Riviere, E. D., Barret, B., Lefevre, F., and Hauchecorne, A.: Remote sensing measurements in the polar vortex: comparison to in situ observations and implications for the simultaneous retrievals and analysis of the NO₂ and OCIO species, *J. Geophys. Res.*, 112, D21310, doi:10.1029/2007JD008699, 2007. 3514, 3523, 3533

25 Damiani, A., Funke, B., Marsh, D. R., López-Puertas, M., Santee, M. L., Froidevaux, L., Wang, S., Jackman, C. H., von Clarmann, T., Gardini, A., Cordero, R. R., and Storini, M.: Impact of January 2005 solar proton events on chlorine species, *Atmos. Chem. Phys. Discuss.*, 12, 1935–1978, doi:10.5194/acpd-12-1935-2012, 2012.

Farman, J. C., Gardiner, G., and Shanklin, J. D.: Large losses of total ozone in antarctica reveal seasonal ClO_x/NO_x interaction, *Nature*, 315, 207–210, 1985. 3513

AMTD

6, 3511–3543, 2013

A global climatology of stratospheric OCIO

C. Tétard et al.

Title Page

Abstract

Introduction

Conclusions

References

Tables

Figures

◀

▶

◀

▶

Back

Close

Full Screen / Esc

Printer-friendly Version

Interactive Discussion



**A global climatology
of stratospheric OCIO**

C. Tétard et al.

Title Page

Abstract

Introduction

Conclusions

References

Tables

Figures

◀

▶

◀

▶

Back

Close

Full Screen / Esc

Printer-friendly Version

Interactive Discussion



- Fussen, D., Vanhellemont, F., Dodion, J., Bingen, C., Mateshvili, N., Daerden, F., Fonteyn, D., Errera, Q., Chabrilat, S., Kyrölä, E., Tamminen, J., Sofieva, V., Hauchecorne, A., Dalaudier, F., Bertaux, J.-L., Renard, J.-B., Fraisse, R., d'Andon, O. F., Barrot, G., Guirlet, M., Mangin, A., Fehr, T., Snoeij, P., and Saavedra, L.: A global OCIO stratospheric layer discovered in GOMOS stellar occultation measurements, *Geophys. Res. Lett.*, 33, L13815, doi:10.1029/2006GL026406, 2006. 3515, 3525
- Hauchecorne, A., Bertaux, J.-L., Dalaudier, F., Russel III, J. M., Mlynczak, M. G., Kyrölä, E., and Fussen, D.: Large increase of NO₂ in the north polar mesosphere in January–February 2004: Evidence of a dynamical origin from GOMOS ENVISAT and SABER TIMED data, *Geophys. Res. Lett.*, 34, L03810, doi:10.1029/2006GL027628, 2007.
- Krecl, P., Haley, C. S., Stegman, J., Brohede, S. M., and Berthet, G.: Retrieving the vertical distribution of stratospheric OCIO from Odin/OSIRIS limb-scattered sunlight measurements, *Atmos. Chem. Phys.*, 6, 1879–1894, doi:10.5194/acp-6-1879-2006, 2006. 3514
- Kühl, S., Pukite, J., Deutschmann, T., Platt, U., and Wagner, T.: SCIAMACHY limb measurements of NO₂, BrO and OCIO, Retrieval of vertical profiles: Algorithm, first results, sensitivity and comparison studies, *Adv. Space Res.*, 42, 1747–1764, 2008. 3514
- Kuttippurath, J., Godin-Beekmann, S., Lefèvre, F., Nikulin, G., Santee, M. L., and Froidevaux, L.: Record-breaking ozone loss in the Arctic winter 2010/2011: comparison with 1996/1997, *Atmos. Chem. Phys.*, 12, 7073–7085, doi:10.5194/acp-12-7073-2012, 2012. 3526
- Kyrölä, E., Tamminen, J., Sofieva, V., Bertaux, J. L., Hauchecorne, A., Dalaudier, F., Fussen, D., Vanhellemont, F., Fanton d'Andon, O., Barrot, G., Guirlet, M., Fehr, T., and Saavedra de Miguel, L.: GOMOS O₃, NO₂, and NO₃ observations in 2002–2008, *Atmos. Chem. Phys.*, 10, 7723–7738, doi:10.5194/acp-10-7723-2010, 2010a.
- Kyrölä, E., Tamminen, J., Sofieva, V., Bertaux, J. L., Hauchecorne, A., Dalaudier, F., Fussen, D., Vanhellemont, F., Fanton d'Andon, O., Barrot, G., Guirlet, M., Mangin, A., Blanot, L., Fehr, T., Saavedra de Miguel, L., and Fraisse, R.: Retrieval of atmospheric parameters from GOMOS data, *Atmos. Chem. Phys.*, 10, 11881–11903, doi:10.5194/acp-10-11881-2010, 2010b. 3517
- Miller, H. L. J., Sanders, R. W., and Solomon, S.: Observations and interpretation of column OCIO seasonal cycles at two polar sites, *J. Geophys. Res.*, 104, 18769–18783, 1999. 3514
- Oetjen, H., Wittrock, F., Richter, A., Chipperfield, M. P., Medeke, T., Sheode, N., Sinnhuber, B.-M., Sinnhuber, M., and Burrows, J. P.: Evaluation of stratospheric chlorine chemistry for the Arctic spring 2005 using modelled and measured OCIO column densities, *Atmos. Chem. Phys.*, 11, 689–703, doi:10.5194/acp-11-689-2011, 2011. 3514

A global climatology of stratospheric OCIO

C. Tétard et al.

Title Page

Abstract

Introduction

Conclusions

References

Tables

Figures

◀

▶

◀

▶

Back

Close

Full Screen / Esc

Printer-friendly Version

Interactive Discussion



Platt, U., Perner, D., and Pätz, H. W.: Simultaneous measurement of atmospheric CH₂O, O₃, and NO₂ by differential optical absorption, *J. Geophys. Res.*, 84, 6329–6335, doi:10.1029/JC084iC10p06329, 1979. 3520

Renard, J. B., Lefevre, F., Pirre, M., Robert, C., and Huguenin, D.: Vertical profile of night-time stratospheric OCIO, *J. Atmos. Chem.*, 26, 65–76, 1997. 3514, 3533

Renard, J. B., Chartier, M., Robert, C., Chalumeau, G., Berthet, G., Pirre, M., and Pommereau, J. P.: SALOMON: a new, light, balloon-borne UV visible spectrometer for nighttime observations of stratospheric trace gas species, *Appl. Optics*, 39, 386–392, 2000. 3514, 3523

Renard, J.-B., Blelly, P.-L., Bourgeois, Q., Chartier, M., Goutail, F., and Orsolini, Y.-J.: Origin of the January–April 2004 increase in stratospheric NO₂ observed in the northern polar latitudes, *Geophys. Res. Lett.*, 33, L11801, doi:10.1029/2005GL025450, 2006.

Riviere, E. D., Pirre, M., Berthet, G., Renard, J. B., Taupin, F. G., Huret, N., and Chartier, M.: On the interaction between nitrogen and halogen species in the Arctic polar vortex during THESEO and THESEO 2000, *J. Geophys. Res.*, 108, 8311, doi:10.1029/2002JD002087, 2003. 3514, 3533

Riviere, E. D., Pirre, M., Berthet, G., Renard, J. B., and Lefevre, F.: Investigating the halogen chemistry from the high-latitude nighttime stratospheric measurements of OCIO and NO₂, *J. Atmos. Chem.*, 48, 261–282, 2004. 3514

Rusch, D. W., Gérard, J. C., and Solomon, S.: The effect of particle precipitation events on the neutral and ion chemistry of the middle atmosphere – I. Odd nitrogen, *Planet. Space Sci.*, 29, 767–774, 1981.

Salawitch, R. J., Wofsy, S. C., Gottlieb, E. W., Lait, L. R., Newman, P. A., Schoeberl, M. R., Loewenstein, M., Podolske, J. R., Strahan, S. E., and Proffitt, M. H.: Chemical loss of ozone in the Arctic polar vortex in the winter of 1991–1992, *Science*, 261, 1146–1149, doi:10.1126/science.261.5125.1146, 1993. 3513

Seppälä, A., Veronen, P. T., Kyrölä, E., Hassinen, S., Backman, L., Hauchecorne, A., Bertaux, J. L., and Fussen, D.: Solar proton events of October–November 2003: Ozone depletion in the northern hemisphere polar winter as seen by GOMOS/Envisat, *Geophys. Res. Lett.*, 31, L19107, doi:10.1029/2004GL021042, 2004.

Sofieva, V. F., Kan, V., Dalaudier, F., Kyrölä, E., Tamminen, J., Bertaux, J.-L., Hauchecorne, A., Fussen, D., and Vanhellefont, F.: Influence of scintillation on quality of ozone monitoring by GOMOS, *Atmos. Chem. Phys.*, 9, 9197–9207, doi:10.5194/acp-9-9197-2009, 2009. 3516

A global climatology of stratospheric OCIO

C. Tétard et al.

Title Page

Abstract

Introduction

Conclusions

References

Tables

Figures

◀

▶

◀

▶

Back

Close

Full Screen / Esc

Printer-friendly Version

Interactive Discussion



Solomon, S.: Stratospheric ozone depletion: A review of concepts and history, *Rev. Geophys.*, 37, 275–316, doi:10.1029/1999RG900008, 1999. 3514

Solomon, S., Garcia, R. R., Rowland, F. S., and Wuebbles, D. J.: On the depletion of antarctic ozone, *Nature*, 321, 755–758, 1986. 3513

5 Solomon, S., Mount, G. H., and Sanders, R.W. Schmeltekopf, A. L.: Visible spectroscopy at McMurdo station, Antarctica 2. Observations of OCIO, *J. Geophys. Res.*, 92, 8329–8338, 1987. 3514

Tétard, C., Fussen, D., Bingen, C., Capouillez, N., Dekemper, E., Loodts, N., Mateshvili, N., Vanhellefont, F., Kyrölä, E., Tamminen, J., Sofieva, V., Hauchecorne, A., Dalaudier, F., Bertaux, J.-L., Fanton d'Andon, O., Barrot, G., Guirlet, M., Fehr, T., and Saavedra, L.: Simultaneous measurements of OCIO, NO₂ and O₃ in the Arctic polar vortex by the GOMOS instrument, *Atmos. Chem. Phys.*, 9, 7857–7866, doi:10.5194/acp-9-7857-2009, 2009. 3514, 3515, 3522

15 Wagner, T., Wittrock, F., Richter, A., Wenig, M., and Burrows, J. P., and Platt, U.: Continuous monitoring of the high and persistent chlorine activation during the Arctic winter 1999/2000 by the GOME instrument on ERS-2, *J. Geophys. Res.*, 107, 8267, doi:10.1029/2001JD000466, 2002. 3514

A global climatology of stratospheric OCIO

C. Tétard et al.

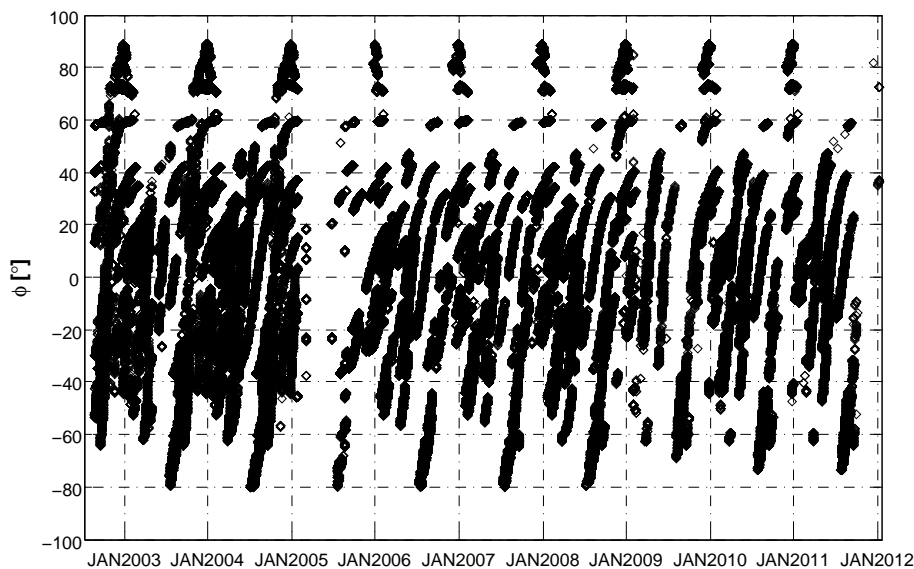


Fig. 1. Example of GOMOS transmittance spectra for an oblique occultation (top panel), a vertical occultation (middle panel) and an averaged occultation (bottom panel). The altitude range is 15 to 60 km.

[Title Page](#)[Abstract](#)[Introduction](#)[Conclusions](#)[References](#)[Tables](#)[Figures](#)[◀](#)[▶](#)[◀](#)[▶](#)[Back](#)[Close](#)[Full Screen / Esc](#)[Printer-friendly Version](#)[Interactive Discussion](#)

A global climatology of stratospheric OCIO

C. Tétard et al.

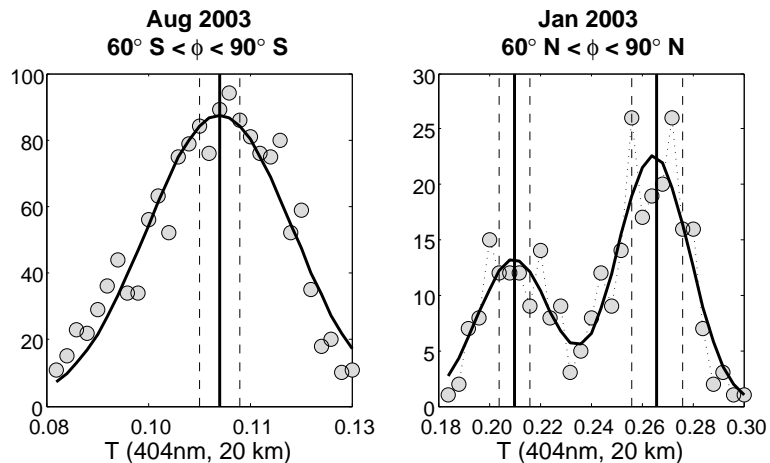


Fig. 2. Latitudinal distribution of the GOMOS measurements selected as a function of time.

[Title Page](#)[Abstract](#)[Introduction](#)[Conclusions](#)[References](#)[Tables](#)[Figures](#)[◀](#)[▶](#)[◀](#)[▶](#)[Back](#)[Close](#)[Full Screen / Esc](#)[Printer-friendly Version](#)[Interactive Discussion](#)

A global climatology of stratospheric OCIO

C. Tétard et al.

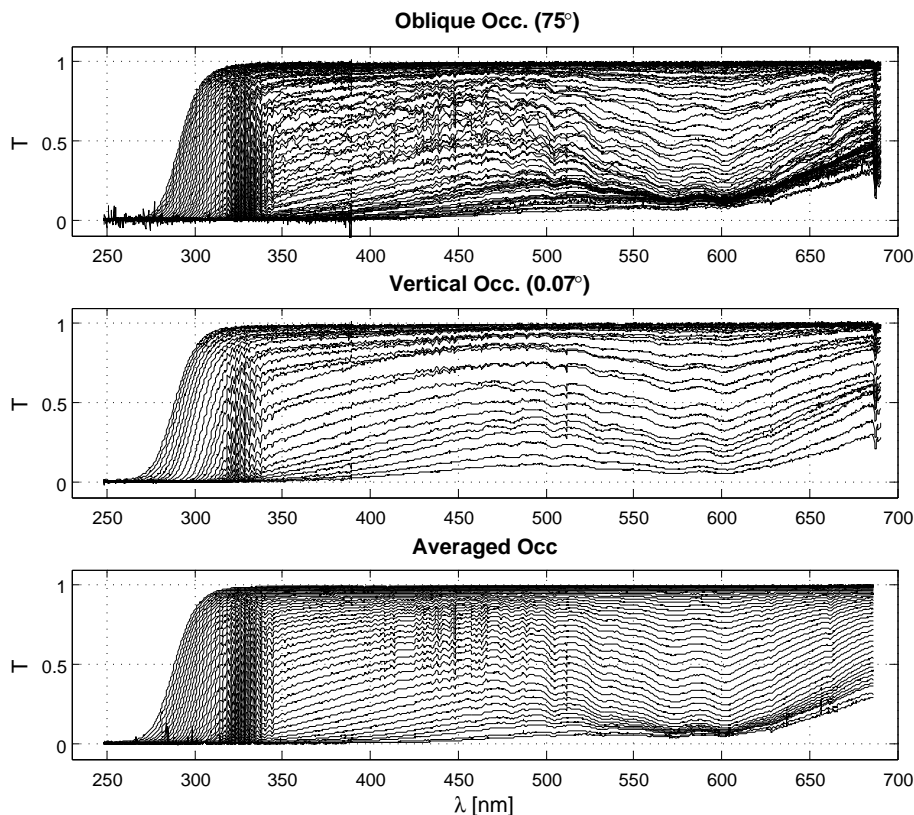


Fig. 3. Example of monomodal (left panel) and bimodal (right panel) distributions of GOMOS transmittance for an altitude of 20 km and a wavelength of 404 nm. The solid curves represent the best fit obtained, the solid vertical lines represent the weighted median for each mode while the dashed lines are the weighted median absolute deviations.

Title Page

Abstract

Introduction

Conclusions

References

Tables

Figures

◀

▶

◀

▶

Back

Close

Full Screen / Esc

Printer-friendly Version

Interactive Discussion



A global climatology of stratospheric OCIO

C. Tétard et al.

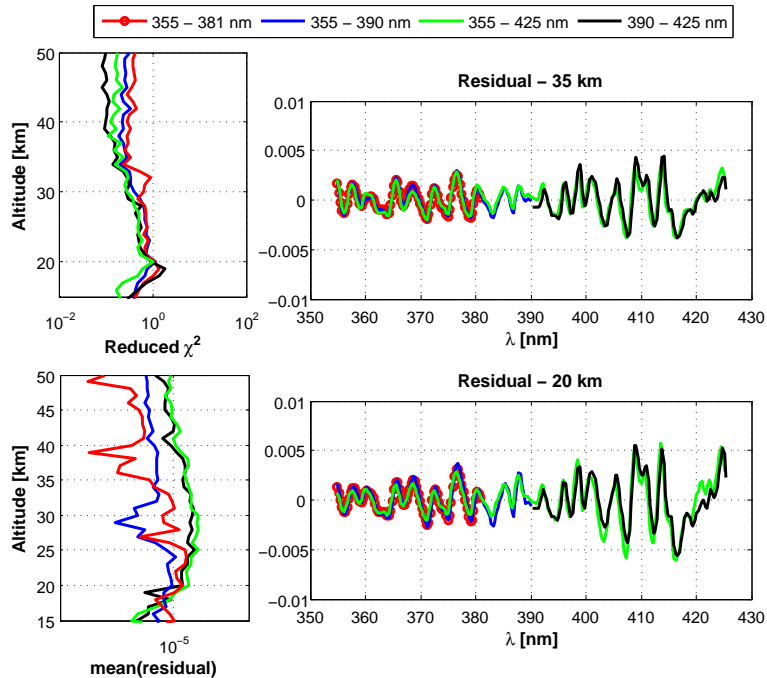


Fig. 4. Left top panel: reduced chi-square as a function of altitude. Left bottom panel: mean of the residual as a function of altitude. Right panel: residual transmittance at 35 and 20 km. These figures show results based on the averaged occultation corresponding to the year 2007 in the $[70^\circ; 80^\circ \text{ S}]$ latitude band.

A global climatology of stratospheric OCIO

C. Tétard et al.

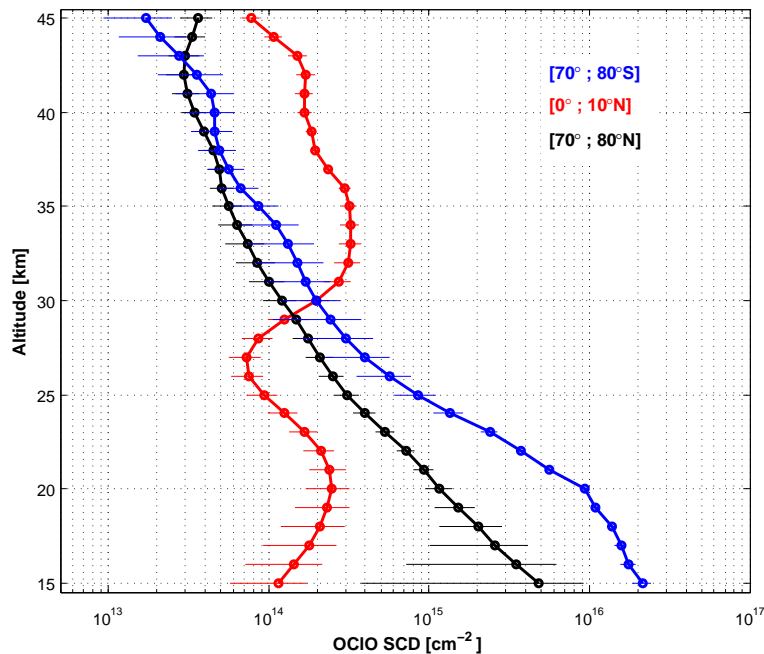


Fig. 5. OCIO SCD profiles retrieved from GOMOS averaged transmittance for the year 2003 in the Antarctic region (in blue), the Arctic region (in black) and in the equatorial region (in red).

[Title Page](#)[Abstract](#)[Introduction](#)[Conclusions](#)[References](#)[Tables](#)[Figures](#)[◀](#)[▶](#)[◀](#)[▶](#)[Back](#)[Close](#)[Full Screen / Esc](#)[Printer-friendly Version](#)[Interactive Discussion](#)

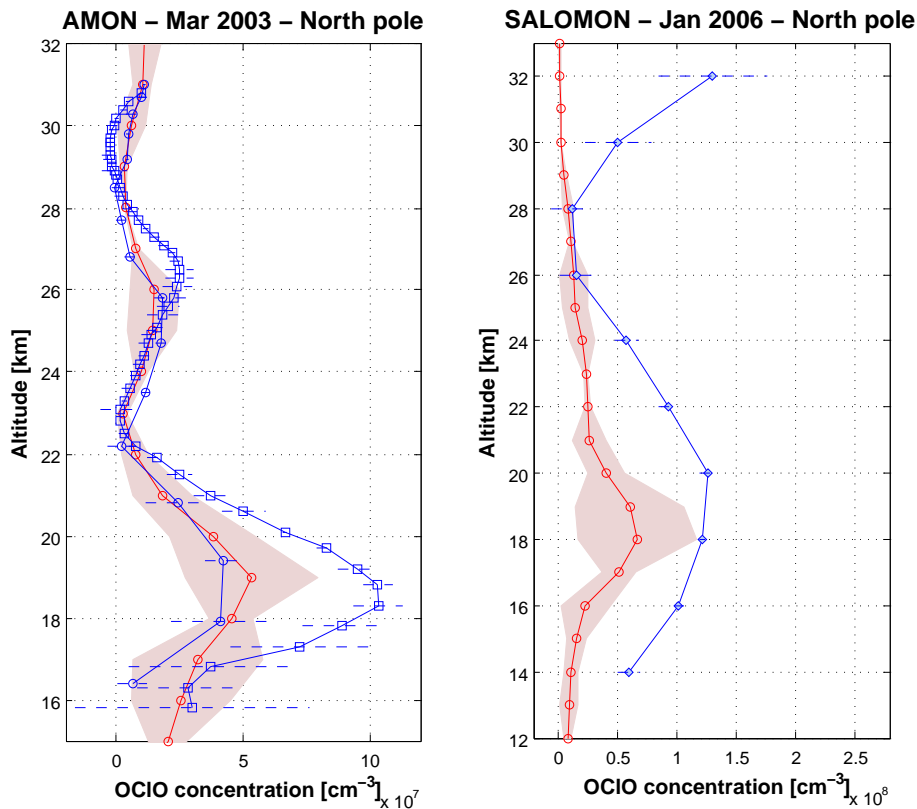


Fig. 6. Left panel: vertical profiles of OCIO concentrations retrieved from GOMOS averaged measurements (in red) and from AMON measurements on 1 March 2003 (blue square for α CMA occultation and circle for ϵ ORI occultation). Right panel: comparisons with a SALOMON measurement (in blue) on 16 January 2006. The shaded area and the horizontal bars represent the associated errors.

Title Page	
Abstract	Introduction
Conclusions	References
Tables	Figures
◀	▶
◀	▶
Back	Close
Full Screen / Esc	
Printer-friendly Version	
Interactive Discussion	



A global climatology of stratospheric OCIO

C. Tétard et al.

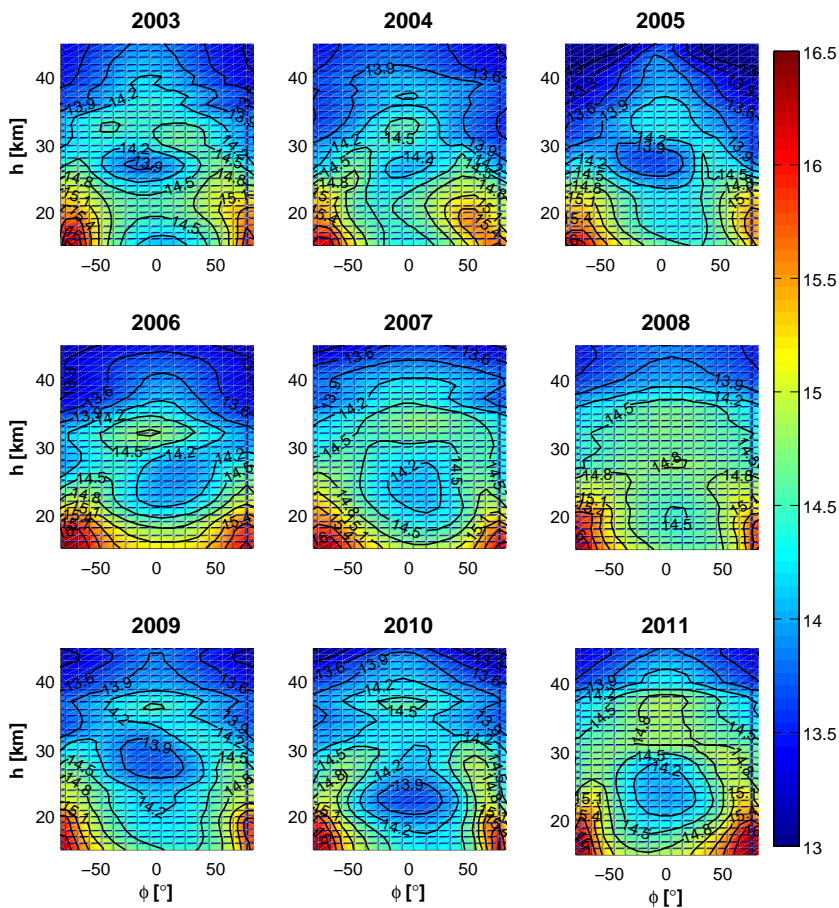


Fig. 7. Latitude-altitude maps of OCIO slant column densities (log scale, cm^{-2}) retrieved from GOMOS measurements for years 2003 to 2011.

[Title Page](#)[Abstract](#)[Introduction](#)[Conclusions](#)[References](#)[Tables](#)[Figures](#)[◀](#)[▶](#)[◀](#)[▶](#)[Back](#)[Close](#)[Full Screen / Esc](#)[Printer-friendly Version](#)[Interactive Discussion](#)

A global climatology of stratospheric OCIO

C. Tétard et al.

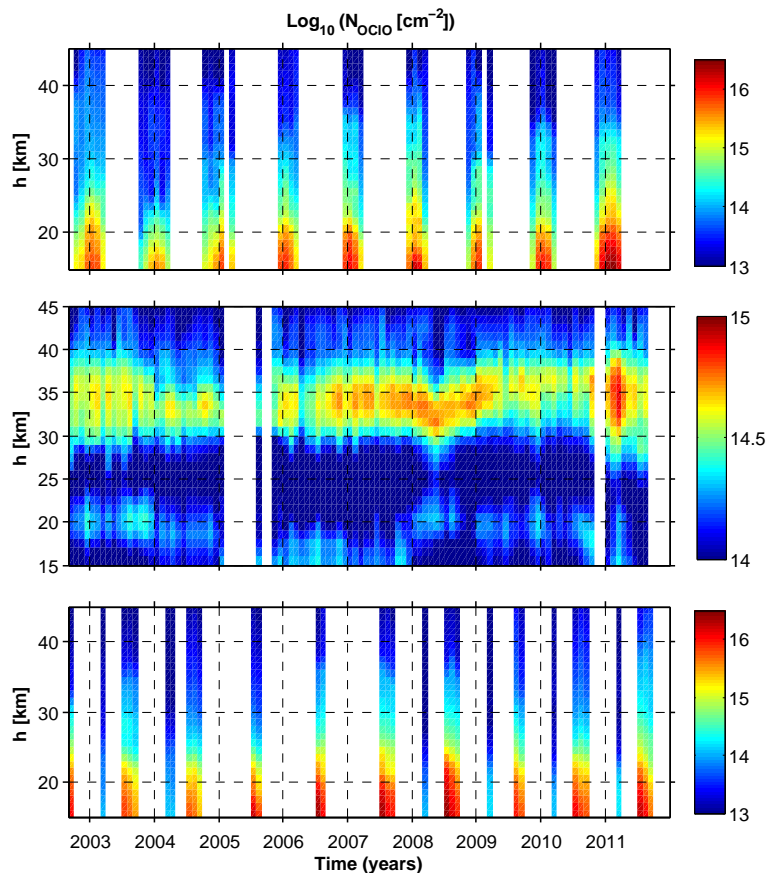


Fig. 8. Monthly OCIO slant column densities (cm^{-2}) in three latitude bands for the period from September 2002 to December 2011. Latitude bands: 60° N–90° N (top panel), 10° S–10° N (middle panel) and 60° S–90° S (bottom panel). The colorscales used are the same for the two polar time series but differs for the equatorial time series.

[Title Page](#)[Abstract](#)[Introduction](#)[Conclusions](#)[References](#)[Tables](#)[Figures](#)[◀](#)[▶](#)[◀](#)[▶](#)[Back](#)[Close](#)[Full Screen / Esc](#)[Printer-friendly Version](#)[Interactive Discussion](#)

A global climatology of stratospheric OCIO

C. Tétard et al.

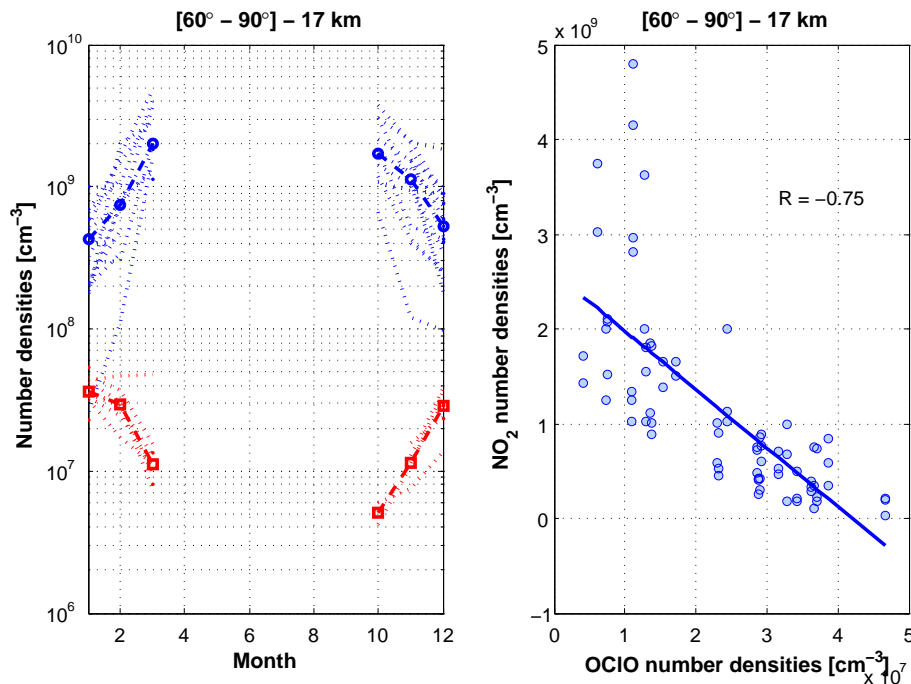


Fig. 9. Left panel: time series of monthly concentrations (molec cm⁻³) of OCIO (red) and NO₂ (blue) in the 60°–90° latitude band for the year 2003 to 2011. The solid lines are the median concentrations. Right panel: Correlation plot of concentrations of OCIO versus NO₂ (molec cm⁻³) at 17 km in the Arctic region. The straight line is the result of a linear least-squares regression (the correlation coefficient is indicated on the plot).

[Title Page](#)[Abstract](#)[Introduction](#)[Conclusions](#)[References](#)[Tables](#)[Figures](#)[◀](#)[▶](#)[◀](#)[▶](#)[Back](#)[Close](#)[Full Screen / Esc](#)[Printer-friendly Version](#)[Interactive Discussion](#)

A global climatology of stratospheric OCIO

C. Tétard et al.

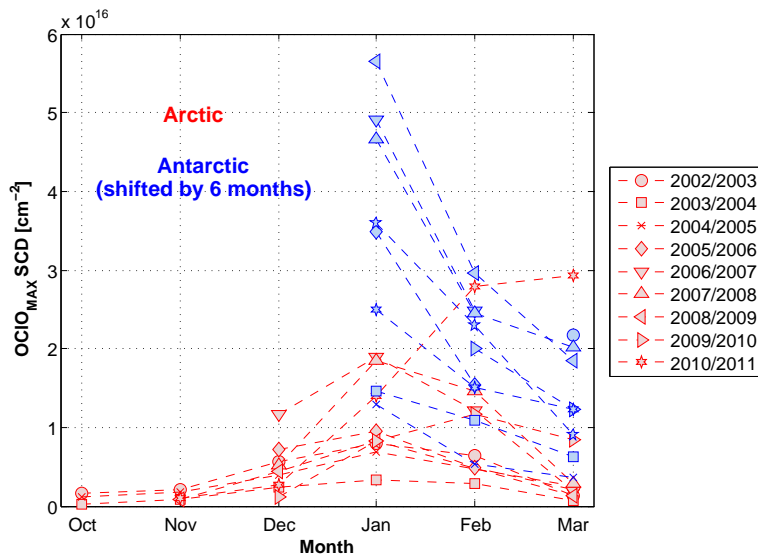


Fig. 10. Maximum monthly OCIO SCDs in the Arctic regions (in red) and in the Antarctic regions (in blue) for the winters 2003 to 2011. For comparisons with the Arctic OCIO SCDs, the Antarctic OCIO values have been shifted by 6 months.

Title Page

Abstract

Introduction

Conclusions

References

Tables

Figures

◀

▶

◀

▶

Back

Close

Full Screen / Esc

Printer-friendly Version

Interactive Discussion

